Polarization of light meromyosin using transient electric birefringence

ARTICLE *in* THE JOURNAL OF PHYSICAL CHEMISTRY · MAY 1992

Impact Factor: 2.78 · DOI: 10.1021/j100190a092

These equations can be solved for the f_k''

$$f_0'' = c\frac{x^2 - x^1}{\Delta_T^0} \quad (17)$$

$$f_1'' = c\frac{x^2 - x^0}{\Delta_T^1} \quad (18)$$

$$f_2'' = c\frac{x^1 - x^0}{\Delta_T^2} \quad (19)$$

where c is some constant. Therefore, the geometry of the phase diagram determines the second derivatives of the free energy in the three coexisting phases up to a scale factor. This is similar to mixtures of three or more components where, at constant pressure *and* temperature, the second derivatives of the free energy are also determined by the phase diagram up to a constant factor.[9,10] If, as is often the case in solid mixtures, a phase has a well-defined stoichiometry, its f'' is very large and its Δ_T very small. On the other hand, a liquid phase which is near-critical or contains large aggregates has a very small f'' and displays a large jump in slope Δ_T.

From eqs 17-19 and the positivity of the f_k'', it follows that all the Δ_T^k must have the same sign. This is equivalent to the 180° rule, which can be stated in the following form:[11] No stable phase may occupy more than 180° of angle at a triple point.

Note we come to the announced constraints on the phase diagram. The temperature plays no special role in the preceding arguments. The p–x diagrams at constant temperature have the same characteristics as the T–x diagrams at constant pressure. Repeating these arguments with the pressure instead of the temperature, we obtain a similar set of equations

$$f_0'' = c'\frac{x^2 - x^1}{\Delta_p^0} \quad (20)$$

$$f_1'' = c'\frac{x^2 - x^0}{\Delta_p^1} \quad (21)$$

$$f_2'' = c'\frac{x^1 - x^0}{\Delta_p^2} \quad (22)$$

where the Δ_p^k correspond to eqs 14-16 with T replaced by p and c' is another scale factor. Comparing these with eqs 17-19, we obtain

$$\frac{\Delta_T^0}{\Delta_p^0} = \frac{\Delta_T^1}{\Delta_p^1} = \frac{\Delta_T^2}{\Delta_p^2} \quad (23)$$

These are the constraints mentioned in the title of this paper. They show that the jumps in slope in a T–x diagram Δ_T^k at a triple point are proportional to the corresponding jumps in the p–x diagram Δ_p^k. In a three-dimensional T–p–x diagram, the geometric quantity Δ_T^k/Δ_p^k has the same value in each of the three coexisting phases along the triple line.

We close with a number of remarks.

Written in the form

$$\frac{\Delta_T^0}{\Delta_T^1} = \frac{\Delta_p^0}{\Delta_p^1} \qquad \frac{\Delta_T^0}{\Delta_T^2} = \frac{\Delta_p^0}{\Delta_p^2}$$

the constraints mean that the ratios Δ_T^0/Δ_T^1 and Δ_T^0/Δ_T^2, which are determined by a T–x diagram, have the same numerical value as the corresponding quantities in a p–x diagram. Now there is nothing special with the temperature or the pressure. Diagrams such as Figure 1 or 2 can be recorded for any "field",[12] μ replacing T. Examples of such fields are magnetic or electric fields,[13,14] the chemical potential of a third component, or, if one of the phases is a solid, the stress.[13,15] The corresponding ratios $\Delta_\mu^0/\Delta_\mu^1$, $\Delta_\mu^0/\Delta_\mu^2$ are independent of the nature of the field and depend only on the response of the system determined by the f_k''.

Consider a mixture having two triple points at T_t and $T_{t'}$ as in Figure 2. If the triple points are sufficiently close together, the f_k'' and the slopes will be nearly unchanged. Eliminating the f_k'' from the two sets (eqs 17-19) yields a constraint on the T–x diagram. We do not go into the details.

There exist similar constraints for n-component mixtures near a point of coexistence of $n + 1$ phases.

Acknowledgment. Several discussions with R. Strey and U. Wuerz are gratefully acknowledged. This work was performed in the department of Prof. Kahlweit, whom I thank for his support.

(9) Teubner, M. *J. Chem. Phys.* **1991**, *94*, 4490.
(10) Teubner, M. *J. Chem. Phys.* **1991**, *95*, 5243.
(11) Wheeler, J. C. *J. Chem. Phys.* **1974**, *61*, 4474.
(12) Griffiths, R. B.; Wheeler, J. C. *Phys. Rev.* **1970**, *A2*, 1047.
(13) Callen, H. B. *Thermodynamics*; John Wiley: New York, 1960.
(14) Landau, L. D.; Lifschitz, E. M. *Course of Theoretical Physics*; Pergamon: London, 1960; Vol. 8.
(15) Landau, L. D.; Lifschitz, E. M. *Course of Theoretical Physics*; Pergamon: London, 1960; Vol. 7.

Polarization of Light Meromyosin Using Transient Electric Birefringence

James F. Curry[†] and Sonja Krause*

Department of Chemistry and Center for Biophysics, Rensselaer Polytechnic Institute, Troy, New York 12180
(Received: June 5, 1991; In Final Form: February 3, 1992)

The specific Kerr constant of rabbit skeletal light meromyosin was measured in various buffer systems between pH 8.7 and 9.6 using transient electric birefringence and showed the generally expected decrease with solution conductivity. Analysis of birefringence rise times and field reversal transients showed that this decrease was connected with large changes in what appeared to be a permanent dipole moment. Comparison of the data with some theoretical predictions (O'Konski, C. T.; Krause, S. *J. Phys. Chem.* **1970**, *74*, 3243) indicated that the changes in the specific Kerr constant were most probably due to a slow induced dipole moment resulting from ion atmosphere polarization. The molecule may also have a permanent dipole moment.

Introduction

Electrooptic techniques have been used successfully to demonstrate that the polarization of the counterion atmosphere of polyelectrolytes is one mechanism by which polyelectrolytes such as deoxyribonucleic acids (DNA) and tobacco mosaic virus (TMV) orient in electric fields. These techniques often use a pulsed electric field in the form of a single square wave to partially orient the macromolecules. The rise and decay of the orientation process can be followed via transient electric birefringence (TEB), di-

[†] Present address: GAF Chemicals Corp., 1361 Alps Road, Wayne, NJ 07470.

0022-3654/92/2096-4643$03.00/0

chroism, and other optical methods. After a square electric field pulse is applied to a macromolecular solution, the macromolecules rotate until a steady-state orientation is achieved. This steady-state orientation depends on the applied electric field, the permanent dipole moment, and the electrical polarizability of the macromolecules. After the electric field is turned off, the field-free rotational relaxation time of the macromolecules back to random orientation yields hydrodynamic information about the macromolecules, such as size, shape, and in some cases, flexibility.

In 1957, O'Konski and Haltner,[1] in a TEB study of TMV, found that the steady-state orientation of TMV in an electric field decreased as the conductivity of the solution increased. The strain of TMV studied in this work had no observable permanent dipole moment. TEB studies of DNA, another molecule with no permanent dipole moment, showed the same trend.[2] This decrease of steady-state orientation with increasing solution conductivity is not confined to macromolecules with no permanent dipole moment, however, since studies of bovine serum albumin[3] (BSA), a protein with a measured permanent dipole moment (384 D),[4] have shown the same trend. Furthermore, a number of investigators[5-8] have shown that the strain of TMV studied by O'Konski and Haltner has a small permanent dipole moment.

In O'Konski and Haltner's study on TMV,[1] the steady-state orientation of the molecule, as measured by the calculated specific Kerr constant, was about 50 times larger than expected from electronic and atomic effects. This could not be due to a permanent dipole moment because the steady-state orientation did not change when the electric field was reversed quickly. However, when pulsed sine wave electric fields were applied to the solutions, the steady-state orientation of the TMV decreased rapidly when the frequency of the applied field was increased above 30 kHz. Some calculations were made showing that these effects were consistent with a model that includes the polarizability of the ion atmosphere around the macromolecules, specifically a surface conductivity related to the relatively high local concentrations of counterions even at the low ionic strengths used in these experiments. A theoretical treatment incorporating these ideas was published by O'Konski and Krause.[9] Calculations based on this theoretical treatment[10] showed that the steady-state orientation of the macromolecules should decrease with increasing solution conductivity in the range used for the experiments. In addition, the observed value of the specific Kerr constant of TMV could be calculated.

In Elias and Eden's TEB study of restriction fragments of DNA,[2] both the variation of the steady-state orientation with the contour length of DNA fragments and with the ionic strength of the solution was compared with various theoretical treatments in the literature. No theoretical treatment agreed very well with the experimental plots of polarizability (directly proportional to the specific Kerr constants) versus the logarithm of the ionic strength of added salt. Predictions using theoretical treatments by Oosawa[11] and by Fixman[12,13] showed a decrease of polarizability with increasing ionic strength that was smaller than that observed experimentally; Oosawa's treatment,[11] with the help of an adjustable parameter, appeared to agree more closely with the experimental data. We may note that data for sodium DNA did not fall on the same curve with data for magnesium DNA. This indicates that ionic strength is not the only parameter that affects ion atmosphere polarization. In addition, we may note that the evidence from electric field reversal experiments indicated that the polarization was slow with respect to the speed of electric field reversal.

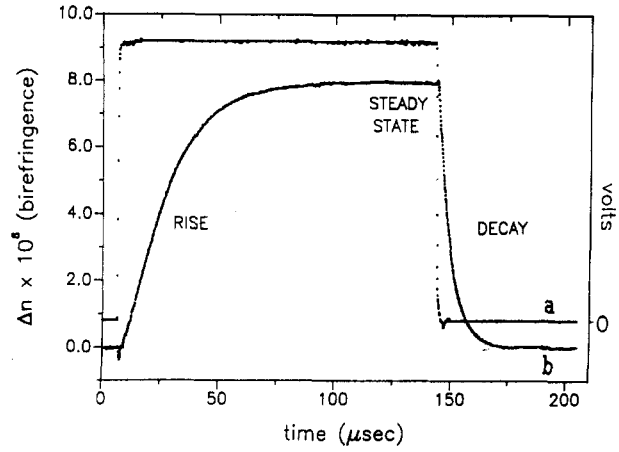

Figure 1. (a) A typical voltage pulse. (b) A typical birefringence signal showing the three regions of the signal.

In the present work, we have studied the steady-state orientation in an electric field of a rigid proteolytic myosin fragment called light meromyosin (LMM) as a function of solution conductivity, that is, as a function of added salt. In our experiments, it first appeared that this rodlike molecule had a permanent dipole moment. It was thus of interest to examine the effect of added salt on the reaction field of the dipole as well as on the ion atmosphere polarization. Analysis of our data, however, indicates that the main polarization mechanism of LMM is a large slow induced dipole moment, most probably connected with ion atmosphere polarization.

Theory

The technique of TEB and its application to macromolecules in solution is described in detail elsewhere.[14-20] Anisometric or electrically anisotropic molecules tend to be oriented in an applied electric field. When plane-polarized light, with its plane of polarization at 45° to the applied electric field, is passed through a solution of the partially oriented molecules, birefringence will be observed if the components of the light parallel and perpendicular to the applied field traveling along the same path have different velocities. This leads to a phase difference given by

$$\delta = \frac{2\pi l}{\lambda}(n_{\parallel} - n_{\perp}) \tag{1}$$

where δ is the phase difference or retardation, in radians, of the two components, l is the path length through the birefringent medium, λ is the wavelength of the incident light in vacuo, and $n_{\parallel}$ and $n_{\perp}$ are the refractive indices of the solution parallel and perpendicular to the direction of the electric field. The birefringence, Δn, is

$$\Delta n = n_{\parallel} - n_{\perp} \tag{2}$$

Application of a rectangular electric field pulse to a solution of macromolecules results in a transient electric birefringence

(1) O'Konski, C. T.; Haltner, A. J. *J. Am. Chem. Soc.* **1957**, *79*, 5634.
(2) Elias, J. G.; Eden, D. *Macromolecules* **1981**, *14*, 410.
(3) Krause, S.; O'Konski, C. T. *J. Am. Chem. Soc.* **1959**, *81*, 5082.
(4) Moser, P.; Squire, P. G.; O'Konski, C. T. *J. Phys. Chem.* **1966**, *70*, 744.
(5) Newman, J.; Swinney, H. L. *Biopolymers* **1976**, *15*, 301.
(6) Jennings, B. R.; Jerrard, H. G. *J. Phys. Chem.* **1966**, *44*, 1291.
(7) Thurston, G. B.; Bowling, D. I. *J. Colloid Interface Sci.* **1969**, *30*, 34.
(8) Ogawa, S.; Oka, S. *J. Phys. Soc. Jpn.* **1960**, *15*, 658.
(9) O'Konski, C. T.; Krause, S. *J. Phys. Chem.* **1970**, *74*, 3243.
(10) Krause, S.; Zvilichovsky, B.; Galvin, M. E. *Biophys. J.* **1980**, *29*, 413.
(11) Oosawa, F. *Biopolymers* **1970**, *9*, 677.
(12) Fixman, M. *J. Chem. Phys.* **1980**, *72*, 5177.
(13) Fixman, M. *Macromolecules* **1980**, *13*, 711.
(14) Yoshioka, K.; Watanabe, H. In *Physical Principles and Techniques of Protein Chemistry, Part A*; Leach, A. S., Ed.; Academic Press: New York, 1969; p 335.
(15) O'Konski, C. T., Ed. *Molecular Electro-Optics*; Marcel Dekker: New York, 1976; Vo. 1, 2.
(16) Fredericq, E.; Houssier, C. *Electric Dichroism and Electric Birefringence*; Clarendon Press: Oxford, UK, 1973.
(17) Jennings, B. R., Ed. *Electro-Optics and Dielectrics of Macromolecules and Colloids*; Plenum Press: New York, 1979.
(18) Krause, S., Ed. *Molecular Electro-Optics*; Plenum Press: New York, 1981.
(19) Eden, D.; Elias, J. G. In *Measurement of Suspended Particles by Light Scattering*, Dahneke, B. E., Ed.; Wiley Interscience: New York, 1983; p 401.
(20) Watanabe, H., Ed. *Dynamic Behavior of Macromolecules, Colloids, Liquid Crystals, and Biological Systems*; Hirokawa Publishing Co.: Tokyo, 1989.

signal. A transient electric birefringence signal can be decomposed into three regions as shown in Figure 1. The rise portion of the signal results when the molecules orient under the influence of the electric field. The steady-state region is attained when the molecules have reached their maximum degree of orientation in the field. The decay is a field-free relaxation of molecules from a partially oriented state back to one of random orientation.

At low electric fields, the specific Kerr constant, K_{sp}, is defined for the steady-state birefringence of the solute

$$K_{sp} = \frac{\Delta n}{nC_v E^2} \tag{3}$$

where n is the refractive index of the unoriented solution, C_v is the volume fraction of solute molecules in solution, and E is the electric field. O'Konski et al.[21] showed that the steady-state birefringence for an ellipsoid of revolution or for any axially symmetric particle at any value of the electric field can be expressed by

$$\Delta n = \frac{2\pi C_v}{n}(g_1 - g_2)\Phi(\beta,\gamma) \tag{4}$$

where $g_1 - g_2$ is the optical anisotropy factor (subscripts 1 and 2 refer to the symmetry and transverse axes of the ellipsoid, respectively), $\Phi(\beta,\gamma)$ is an orientation function which depends on the electric field strength, E, the permanent dipole moment, μ, and the excess electric polarizability, $\alpha_1 - \alpha_2$, of the orienting molecule. At low electric field strengths, the orientation factor for a particle with μ directed along the symmetry axis is

$$\Phi(\beta,\gamma) = (1/15)(\beta^2 + 2\gamma) \tag{5}$$

which yields an expression for K_{sp}

$$K_{sp} = \frac{2\pi(g_1 - g_2)}{15n^2}(P + Q) \tag{6}$$

where

$$P = (\mu/kT)^2 \tag{7}$$

$$Q = \frac{\alpha_1 - \alpha_2}{kT} \tag{8}$$

In these theoretical expressions, P is a permanent dipole term and Q is the induced dipole term which contains contributions from all induced moments. Therefore, K_{sp} as expressed by eq 6, although derived for an un-ionizable macromolecule in an insulating solution, remains applicable to an ionizable macromolecule (polyelectrolyte) in an ionic solution except that P and Q are not expressed using eqs 7 and 8. Theoretical expressions for P and Q for both insulating and conducting systems are given in the Discussion.

$\Phi(\beta,\gamma)$ is a useful function to consider because as $E \to \infty$, $\Phi(\beta,\gamma) \to 1$ ($\Phi = 1$ implies complete orientation). With the steady state birefringence at infinite field strength denoted by Δn_s (saturation birefringence), eq 4 is reduced to

$$\Delta n_s = \frac{2\pi C_v}{n}(g_1 - g_2) \tag{9}$$

and the birefringence is independent of the electrical properties of the molecule. Δn_s can be determined by extrapolation to infinite field strength on a plot of Δn versus E^{-2}.[21] Once Δn_s is determined, $g_1 - g_2$ can be calculated.

The optical anisotropy of an ellipsoid of revolution was shown by Peterlin and Stuart[22] to depend on the geometry of the macromolecule, the refractive index of the solvent (n_0), and the refractive indices along the symmetry and transverse axis of the molecule (n_1 and n_2, respectively). The optical anisotropy is defined by

$$g_1 - g_2 = \frac{4\pi(n_1^2 - n_2^2) - \dfrac{(n_1^2 - n_0^2)(n_2^2 - n_0^2)}{n_0^2}(L_1 - L_2)}{\left[4\pi + \dfrac{(n_1^2 - n_0^2)}{n_0^2}L_1\right]\left[4\pi + \dfrac{(n_2^2 - n_0^2)}{n_0^2}L_2\right]} \tag{10}$$

L_1 and L_2 are form factors defined by

$$L_1 = (4\pi/3)(1 - 2e) \tag{11}$$

$$L_2 = (4\pi/3)(1 + e) \tag{12}$$

For a prolate ellipsoid, e is given by

$$e = \frac{1}{4(A^2 - 1)}\left[2A^2 + 4 - 3\frac{A}{(A^2 - 1)^{1/2}}\ln\frac{A + (A^2 - 1)^{1/2}}{A - (A^2 - 1)^{1/2}}\right] \tag{13}$$

where A is the axial ratio ($A = a/b \equiv$ length/diameter) of the ellipsoid.

Benoit[23] has shown that the field-free decay of birefringence of a dilute monodisperse axially symmetric system is given by

$$\Delta n = \Delta n_0 e^{-6\theta t} \tag{14}$$

where Δn_0 is the initial value of the birefringence at time $t = 0$, when the electric field is turned off. θ is the rotational diffusion coefficient of the macromolecule and can be represented by rotation of the molecule about its minor axes. For a macromolecule modeled as a long cylindrical rod, the original Broersma[24] equation is

$$\theta = \frac{3kT}{8\pi\eta a^3}\left[\ln\frac{2a}{b} - 1.57 + 7\left(\frac{1}{\ln\dfrac{2a}{b}} - 0.28\right)^2\right] \tag{15}$$

where θ is in s^{-1}, η is the viscosity of the solvent in poise, and $2a$ and $2b$ are the length and diameter of the rod, respectively. Broersma[25] later corrected his equation for the case of cylinders with much larger axial ratios than LMM, and Tirado and García de la Torre[26] have developed a more accurate method of calculating θ for cylinders, but eq 15 gives reasonable results in closed form and can be used to show that the rotational diffusion coefficient depends on the dimensions of the molecule and is roughly proportional to the inverse third power of the length. The relaxation time, τ, is related to the rotational diffusion coefficient by

$$\tau = 1/6\theta \tag{16}$$

τ can be substituted into eq 14 to express the birefringence as a function of time to give

$$\Delta n = \Delta n_0 e^{-t/\tau} \tag{17}$$

The relaxation time, by definition, is the time it takes for the initial birefringence signal, Δn_0 (when the field is turned off), to decay to $1/e$ of its initial value. The calculated rotational diffusion coefficient along with eq 16 can be used to predict the relaxation time of a rodlike molecule of a given length and axial ratio.

For a polydisperse system of very anisometric molecules, the decay of the birefringence is multiexponential, and if there is a discrete distribution of molecular lengths, the decay takes the form

$$\Delta n = \sum_i \Delta n_{0,i} e^{-t/\tau_i} \tag{18}$$

(21) O'Konski, C. T.; Yoshioka, K.; Orttung, W. H. *J. Phys. Chem.* **1959**, *63*, 1558.

(22) Peterlin, A.; Stuart, H. A. *Doppelbrechung insbesondere künstliche Doppelbrechung*, In *Hand-und-Jahrbuch der chemischen Physik*; Eucken, A., Wolf, K. L., Ed.; Akademische Verlaggesellschaft: Leipzig, 1943; Vol. 8, Part 1B.

(23) Benoit, H. *Ann. Phys.* **1951**, *6*, 561.

(24) Broersma, S. *J. Chem. Phys.* **1960**, *32*, 1626.

(25) Broersma, S. *J. Chem. Phys.* **1981**, *74*, 6989.

(26) Tirado, M. M.; García de la Torre, J. *J. Chem. Phys.* **1980**, *73*, 1986.

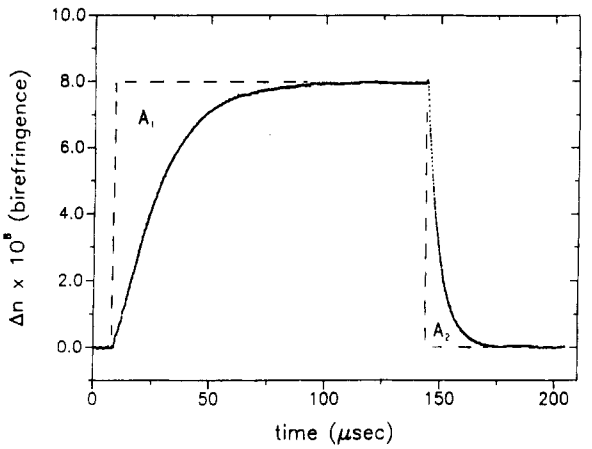

Figure 2. Areas, A_1 and A_2, bounded by the birefringence rise and decay curves.

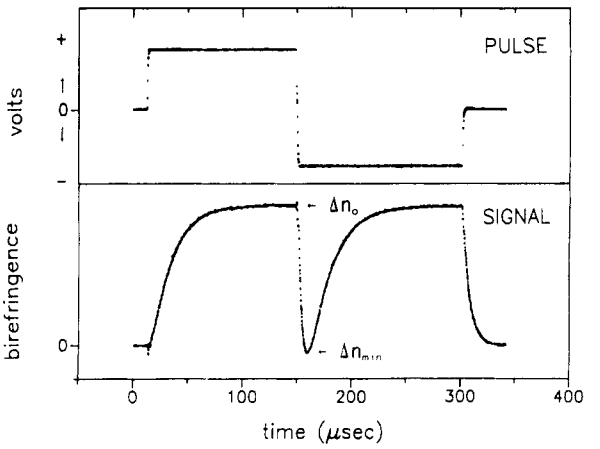

Figure 3. Reversing pulse and corresponding birefringence signal.

where $\Delta n_{0,i}$ is the contribution to the steady-state birefringence originating from the ith species at time zero and τ_i its relaxation time. Curve fitting routines such as DISCRETE[27,28] have been used[29] to analyze birefringence decay data in terms of a discrete sum of exponential decays. If a macromolecule is flexible, multiple relaxation times may correspond to the relaxation of segments as opposed to the whole molecule. Some workers have calculated[30,31] multiple relaxation times which could result from flexible molecules modeled as a series of rigid segments connected by flexible joints. In the case of a rodlike molecule, if a single relaxation time is observed and is less than that predicted using an appropriate model (such as the Broersma equation), then the rodlike coil is generally assumed flexible.

In the case of insulating systems, it is possible to experimentally determine P/Q by measuring the areas under the rise and decay curves. As will be explained below, when we have charged macromolecules in conducting solutions, the values of P and Q obtained from the transients in the birefringence data may not be the same as those that are applicable to the steady-state data. Therefore, the P and Q applicable to transient data will be called P^* and Q^* from this point onward in this paper. Yoshioka and Watanabe[32] showed that the areas bounded by the rise and decay curves, A_1 and A_2, respectively, are related to P^*/Q^* by

$$\frac{A_1}{A_2} = \frac{4P^*/Q^* + 1}{P^*/Q^* + 1} \tag{19}$$

These areas are shown in Figure 2. When $P^*/Q^* \to \infty$, this implies a negligible contribution from the transient induced dipole term, Q^*. When $P^*/Q^* \to 0$, this implies a negligible contribution from the transient permanent dipole term, P^*. The determination of P^*/Q^* using A_1 and A_2 will be referred to as the area method. P^*/Q^* may also be determined using a reversing pulse technique. This technique is performed by applying two pulses of equal voltage but opposite polarity. A theory for the birefringence using a reversing pulse has been developed by Tinoco and Yamaoka[33] for elongated ellipsoids at limiting low fields. A transient in the birefringence will be observed upon field reversal if there is a nonzero P^* term. This will occur *both* when a permanent dipole moment is present in the macromolecule ($P \neq 0$) *and* when the polarization of the ion atmosphere is slow with respect to the time of field reversal. When there is a permanent dipole moment in the macromolecule, it must rotate to reorient in the opposite field direction. When there is a slow induced dipole contribution to the orientation due to ion atmosphere polarization, the rotation of the macromolecule is coupled to this effect, and a transient in the birefringence will also be observed.[33] The transient, no matter what its cause, is related to P^*/Q^* by

$$\frac{P^*}{Q^*} = \frac{1 - \Delta n_{min}/\Delta n_0}{0.1547 + \Delta n_{min}/\Delta n_0} \tag{20}$$

where Δn_{min} is the birefringence at the minimum in the transient and Δn_0 is the steady-state birefringence. A reversing pulse and birefringence signal are shown in Figure 3. The determination of P^*/Q^* from the reversing pulse technique will be referred to as the RP method.

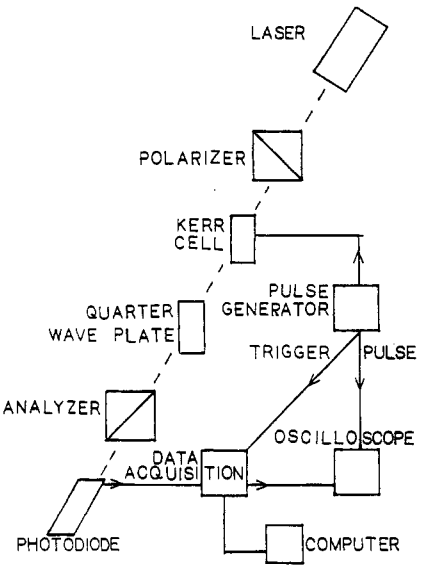

Figure 4. Schematic of electric birefringence apparatus.

Experimental Section

A schematic of the birefringence apparatus is shown in Figure 4. The light source was a 15-mW He–Ne laser, Spectra-Physics Model 124B, operating at 632.8 nm. The polarizer was a Glan Taylor prism designed for 632.8-nm light from a moderately powered laser. The prism was oriented so that the incoming beam was plane polarized at an angle of 45° with respect to the direction of the electric field. The Kerr cell was a copper block machined to thermostatically house a 1-cm quartz cuvette along with the electrodes. The Kerr cell had entrance and exit slits to allow the light beam to pass through and had hollowed out sections through which water was circulated to control temperature. An Omega type 100-W30 platinum RTD element inserted into the cuvette was used to monitor the temperature. Using a Haake Model Fe temperature control reservoir, temperature between 4 and 80 °C could be obtained. Quartz cuvettes which did not exhibit any strain birefringence were selected for this work.

The electrodes were two sheets of platinum (1 × 9 × 50 mm) held vertically in the quartz cuvette using a Bakelite holder.

(27) Provencher, S. W. *J. Chem. Phys.* **1976**, *64*, 2772.
(28) Provencher, S. W. *Biophys. J.* **1976**, *16*, 27.
(29) Lewis, R. J.; Pecora, R.; Eden, D. *Macromolecules* **1986**, *19*, 134.
(30) Wegener, W. A. *Biopolymers* **1982**, *21*, 1049.
(31) Garcia de la Torre, J.; Bloomfield, V. A. *Biochemistry* **1980**, *19*, 5118.
(32) Yoshioka, K.; Watanabe, H. *J. Chem. Soc. Jpn.* **1963**, *84*, 626.
(33) Tinoco, I.; Yamaoka, K. *J. Phys. Chem.* **1959**, *63*, 423.

Previously designed,[34] this holder secured the electrodes parallel to each other and held them firmly into the copper block. The electrode separation distance and the path length of the electrodes were 2.30 ± 0.05 mm and 9.20 ± 0.05 mm, respectively. The quarter-wave plate was an Oriel Model 25820, zero-order quartz plate design for 632.8-nm light. The plate was oriented with its slow axis at 135° to the direction of the electric field. The analyzer was another Glan Taylor prism, identical to the polarizer. A lens was placed after the analyzer to focus the light beam onto the photodiode. The photodiode was a United Detector Technology Model UDT 455HS-Photop PIN photodiode. An additional amplifier was used to increase the gain and provide additional dc offset. The output of this amplifier was sent to a Nicolet LAS (NLAS) 1270 data acquisition system. The NLAS was a 20-MHz, 8-bit, A/D converter, with dual channel capabilities. The NLAS was used to capture and store simultaneous pulse and birefringence signals. One frequently used function of the NLAS was signal averaging. Most signals were averaged 4, 9, or 16 times to improve the signal to noise ratio. The NLAS communicated with an IBM PC using RS-232 connections. The birefringence signal, the electric field pulse signal, and the signal parameters were transferred to the PC.

The voltage pulse was produced using a Cober 605P high-power pulse generator. The reversing pulse was produced using two generators coupled in parallel so that the falling edge of a positive going pulse was coincident with the rising edge of a negative going pulse. The response time of the photodiode, 1.0 μs, was obtained by measuring the birefringence decay signal of water. The Kerr constant of water measured in this work was 2.8×10^{-14} m/V^2 in good agreement with a previously reported value[35] of 2.96×10^{-14} m/V^2.

LMM is composed of two protein chains wound as a coiled coil of α-helices and has an approximate molecular weight of 1.4×10^5 g/mol.[36] LMM was prepared in the laboratory of W. F. Harrington at Johns Hopkins University by digestion of myosin with trypsin as reported by Lowey[37] and summarized by Margossian.[36] The LMM was transported on ice to our laboratory, freeze dried from a 10 mM PP_i solution, and stored at 0 °C. LMM solutions were prepared by dissolving the protein in four buffer systems prepared from the following: tetrasodium pyrophosphate (PP_i), 3-[cyclohexylamino]-2-hydroxy-1-propanesulfonic acid (CAPSO), 2-[*N*-cyclohexylamino]ethanesulfonic acid (CHES), and potassium phosphate monobasic and dibasic (PO_4). These buffers were chosen for their relatively high electrical resistivity. The LMM solutions were dialyzed against their respective buffers. However, for some of the PP_i solutions, LMM was dissolved directly into the solution. The LMM solutions were initially centrifuged at 100 000*g* for at least 1 h. However, since LMM solutions which were filtered through membrane (Millipore HVLP, 0.45 μm, 13 mm diameter) were not measurably different in K_{sp} or τ, centrifugation was discontinued and filtration was used as the method of choice to remove insoluble particles. LMM concentrations were determined by UV absorbance at 280 nm using ϵ_{280} of 0.30 cm^2/mg for LMM.[36] The purity of LMM was determined by sodium dodecyl sulfate poly(acrylamide) gel electrophoresis, SDS PAGE. Figure 5 shows a typical gel of LMM. Lane a contained standards obtained from Bio-Rad Laboratories with molecular weights as shown. Lanes b and c contained LMM with lane b intentionally overloaded. Gels of LMM were run occasionally to check for degradation. All gels run showed LMM to be somewhat polydisperse with molecular weights ranging from approximately 5×10^4 to 7×10^4 g/mol.

After the concentration and pH were measured, the quartz cuvette containing the sample was placed into the Kerr cell holder and the solution was allowed to reach thermal equilibrium, usually

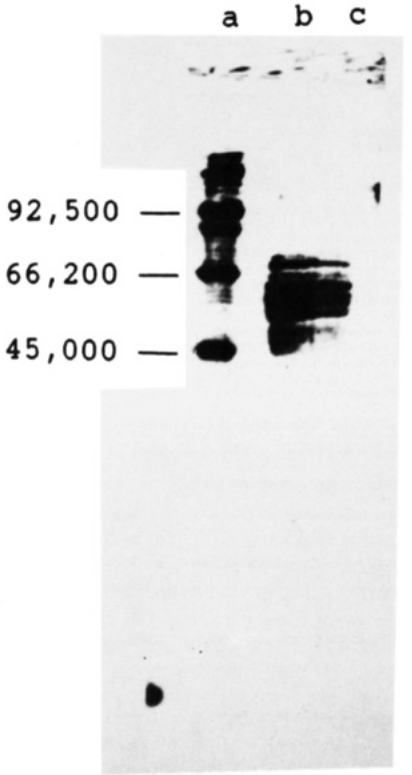

Figure 5. SDS PAGE of LMM.

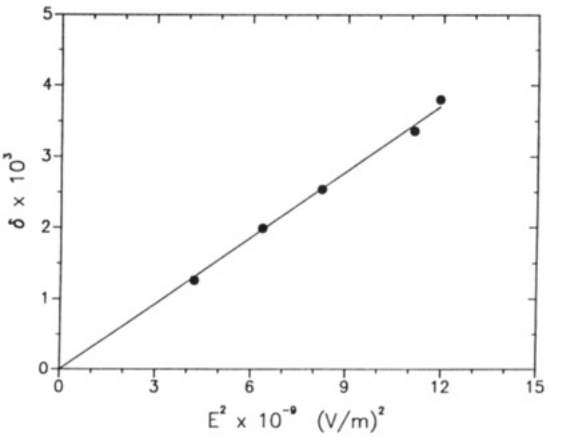

Figure 6. A typical plot of δ versus E^2 for LMM.

at 20 °C. Temperature was controlled and measured to ±0.1 °C. The sample resistance was then measured using a General Radio Co. impedance bridge, Type 650-A. The sample resistance was converted to a conductivity value using the measured resistance and known conductivity of a 0.01 M KCl solution. TEB measurements were performed by starting with the lowest field strength which could give a measurable TEB signal. The electric field was increased in steps until at least five ascending field strengths were applied. At least one intermediate field strength was then reapplied to check that no changes in the sample had taken place due to repeated pulsing. The polarity of the electrodes was reversed after each pulse to avoid electrophoretic or polarization effects. Generally, at least four TEB signals were averaged at any particular field strength. The birefringence pulses shown in Figures 1 and 2 are typical averaged pulses of our LMM samples. The data discussed in this paper were all based on birefringence pulses that had a definite steady-state birefringence and that returned to zero birefringence at the end of the birefringence decay. Upon completion of pulsing a particular sample, the resistance and pH were remeasured to check that repetitive voltage pulsing had not deteriorated the protein solution. Occasionally, the concentration of LMM was also remeasured after pulsing. There were never any significant differences in resistance, pH, or concentration

(34) DeLaney, D. E. Ph.D. Thesis 1975, Rensselaer Polytechnic Institute, Troy, NY.
(35) Aroney, M. J.; Battaglia, M. R.; Ferfoglia, R.; Millar, D.; Pierens, R. K. *J. Chem. Soc., Faraday Trans. 2* **1976**, *72*, 724.
(36) Margossian, S. S.; Lowey, S. In *Methods in Enzymology*; Colowick, S. P., Kaplan, N. O., Eds.; Academic Press: New York, 1982; Vol. 84, p 55.
(37) Lowey, S.; Cohen, C. *J. Mol. Biol.* **1962**, *4*, 293.

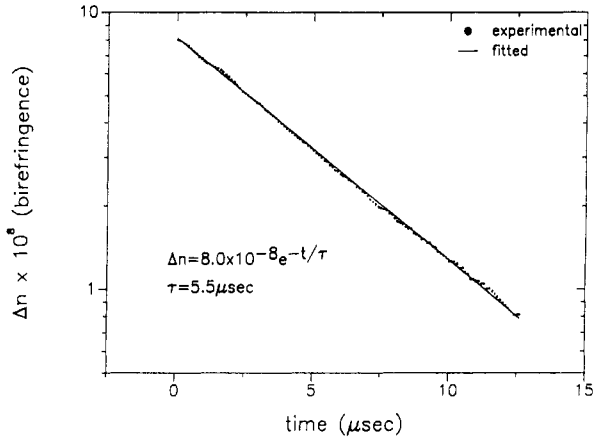

Figure 7. A semilog plot of birefringence versus time for LMM.

measured before and after pulsing.

The specific Kerr constant of a particular sample was determined from a plot of δ versus E^2, where δ is obtained from the steady-state region of the TEB signal. The slope of this line was determined from least-squares analysis of the data. A plot of δ versus E^2 is shown in Figure 6 for LMM in 2 mM PP_i, 0.3 mM HCl at 0.75 mg/mL. The specific Kerr constant was calculated using eq 3, which also required the volume fraction of the sample which was determined from the measured concentration and the partial specific volume. A previously reported value of the partial specific volume of 0.70 cm^3/g for LMM[38] was used. All measurements for which K_{sp} is reported in this paper were done at 20 °C.

For an LMM birefringence decay, log Δn versus time was plotted and if the decay was monoexponential, a best straight line through the data could be obtained. The relaxation time was then calculated from the slope of the line using eq 17. A typical semilog plot of Δn versus time for LMM is shown in Figure 7. The fitted line was calculated using DISCRETE. From the relaxation time, the length of LMM could be calculated using eq 16 and the Broersma equation, eq 15, with an assumed molecular diameter of 20 Å. This value of 20 Å seems common to fibrous muscle proteins such as myosin and tropomyosin.[39-42]

Results

Since LMM is obtained from enzymatic digestion in which more than one cleavage site is susceptible to proteolysis, it is not monodisperse and shows multiple bands on an electrophoresis gel as can be seen in Figure 5. In spite of this, our LMM sample exhibited a single relaxation time within experimental error and we have thus treated the data as if it came from a monodisperse sample. The mean relaxation time for those samples of LMM for which data are reported in this work, measured at 20.0 °C in PP_i, CAPSO, CHES, and PO_4 solutions with pH from 8.7 to 9.6, was 5.8 ± 0.2 μs and was independent of LMM concentration between 0.04 and 3.70 mg/mL. This relaxation time is in good agreement with a previously reported LMM relaxation time of 6.4 ± 0.4 μs determined using TEB.[43] The value of 5.8 μs corresponds to a length of 715 Å using eqs 15 and 16, assuming the diameter of 20 Å.

When KCl was added to CHES and CAPSO buffers in order to obtain solutions with increased conductivities, the relaxation time of the dissolved LMM first increased and then became polydisperse. Polydisperse relaxation times were also obtained at pH 4 in CHES buffer and at pH 7 in PP_i and PO_4 buffer. No data are reported for these solutions.

The conductivity dependence of K_{sp} of LMM in the pH ranges 9.4–9.6 and 8.7–9.0 is shown in Figure 8. The conductivity of

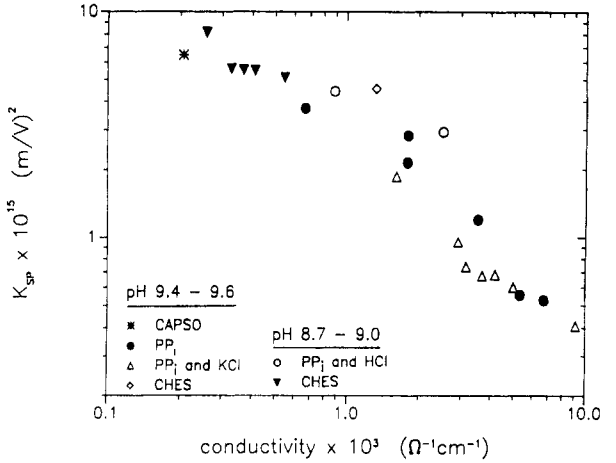

Figure 8. log K_{sp} versus log conductivity for LMM, pH 8.7–9.6.

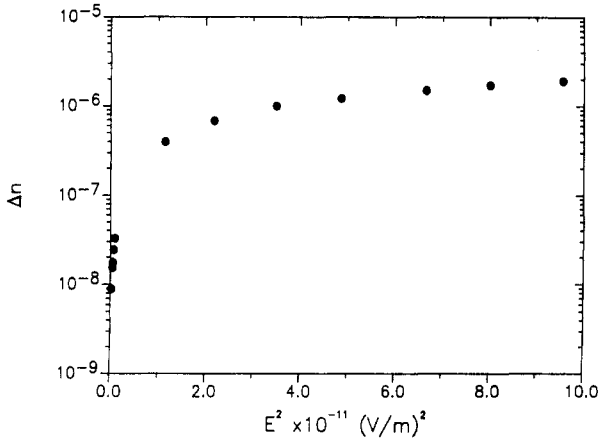

Figure 9. log birefringence versus E^2 approaching saturation for LMM.

the buffered LMM solutions was increased by either increasing the buffer concentration or by adding KCl. Measurements of K_{sp} of LMM in solutions with higher conductivities than 9.11 × 10^{-3} S cm^{-1} (the highest conductivity value on the graph) was not possible because the TEB apparatus could not measure the weak signals produced by these samples, even with signal averaging. Measurements of K_{sp} of LMM in PP_i solutions with lower conductivities than 6.66 × 10^{-4} S cm^{-1} (the lowest conductivity value for LMM in PP_i on the graph, a 2 mM PP_i solution) are not shown because LMM relaxation times were polydisperse or much greater than 5.8 μs in solutions with PP_i concentrations less than 2 mM. Deviations in the relaxation time such as these generally indicate molecular aggregation which prevent the study of K_{sp} of monomeric macromolecules. Lower solution conductivities using CAPSO or CHES were not possible because LMM was not soluble in lower concentrations of these buffers. The K_{sp} of LMM in CHES or CAPSO solutions of higher solution conductivities than those shown in Figure 8 was not calculated since, as stated above, the relaxation times were significantly larger than 5.8 μs and many of the relaxation times were polydisperse.

From the data in Figure 8 it is possible to draw two conclusions: (1) the variation in pH from 8.7 to 9.6, resulting from the various buffer solutions used, did not affect K_{sp}, and (2) the observed decrease in K_{sp} with increasing conductivity is outside experimental error. It can be seen in this figure that the greatest decrease in K_{sp} with increasing conductivity occurs in the conductivity range between approximately 1.0 × 10^{-3} and 1.5 × 10^{-3} S cm^{-1}. In this conductivity range, K_{sp} of LMM also seems to display some buffer dependence.

The optical anisotropy factor for LMM was calculated from the saturation birefringence (Δn_s) of LMM. Measured values of the steady-state birefringence, approaching saturated electric fields, are shown in Figure 9. These data are from a 0.75 mg/mL LMM solution in 2 mM PP_i, 0.3 mM HCl, pH 8.95. The magnitude of Δn_s, determined from a plot of Δn versus $1/E^2$

(38) Young, D. M.; Himmelfarb, S.; Harrington, W. F. *J. Biol. Chem.* **1964**, *239*, 2822.
(39) Lowey, S.; Kucera, J.; Holtzer, A. *J. Mol. Biol.* **1963**, *7*, 234.
(40) Lowey, S. *J. Biol. Chem.* **1965**, *240*, 2421.
(41) Huxley, H. E. *J. Mol Biol.* **1963**, *7*, 281.
(42) Zobel, C. R.; Carlson, F. D. *J. Mol. Biol.* **1963**, *7*, 78.
(43) Cardinaud, R.; Bernengo, J. C. *Biophys. J.* **1985**, *48*, 751.

TABLE I: P^*/Q^* Values Determined from the Area and the RP Method for LMM Samples and the P, Q, μ, and $\alpha_1 - \alpha_2$ Calculated from These P^*/Q^* Values Assuming That $P^*/Q^* = P/Q$

conductivity × 10^3, S cm^{-1}	P^*/Q^*	$P \times 10^{12}$, $(m/V)^2$	$Q \times 10^{12}$, $(m/V)^2$	μ, D	$\alpha_1 - \alpha_2$ × 10^{16}, cm^3	method
0.207	3.2 ± 0.2	13.6	4.3	4400	1.52	area
0.207	21 ± 3	17.0	0.81	5000	0.29	RP
0.258	12.7 ± 0.6	20.8	1.64	5500	0.59	area
0.258	∞	22.5	zero	5700	0	RP
0.328	9.3 ± 1.0	14.0	1.50	4500	0.54	area
0.369	2.60 ± 0.06	11.0	4.24	3990	1.51	area
0.412	29.0 ± 0.2	14.7	0.506	4610	0.181	area
0.548	6.0 ± 0.3	12.1	2.0	4500	0.72	area
0.666	1.11 ± 0.04	5.70	5.14	2790	1.75	area
0.666	6.8 ± 0.3	8.9	1.31	3600	0.47	RP
0.886	6.2 ± 0.1	10.5	1.70	3900	0.60	area
0.886	8.8 ± 1.1	11	1.2	4000	0.44	RP
1.32	2.5 ± 0.1	9.0	3.6	3600	1.27	area
1.32	21 ± 3	12.0	0.57	4200	0.20	RP
1.61	0.82 ± 0.04	2.31	2.82	1830	1.00	area
1.61	1.9 ± 0.2	3.4	1.7	2200	0.62	RP
1.79	1.55 ± 0.17	3.6	2.3	2300	0.82	area
1.80	0.86 ± 0.16	3.6	4.2	2300	1.5	area
2.52	0.92 ± 0.06	3.86	4.19	2360	1.49	area
2.92	1.2 ± 0.3	1.4	1.2	1400	0.42	area
3.16	1.2 ± 0.2	1.1	0.9	1300	0.33	area
3.53	0.59 ± 0.06	1.22	2.08	1320	0.75	area
3.53	1.7 ± 0.1	2.1	1.2	1700	0.44	RP
3.69	0.85 ± 0.12	0.8	1.0	1100	0.36	area
3.69	1.82	1.20	0.66	1320	0.235	RP
4.18	0.58 ± 0.05	0.69	1.18	1000	0.42	area
4.18	1.88	1.22	0.65	1330	0.232	RP
4.99	0.79 ± 0.09	0.73	0.92	1020	0.33	area
4.99	2.15	1.13	0.52	1280	0.187	RP
5.33	0.219 ± 0.004	0.274	1.25	620	0.450	area
6.72	0.23 ± 0.04	0.27	1.18	610	0.422	area

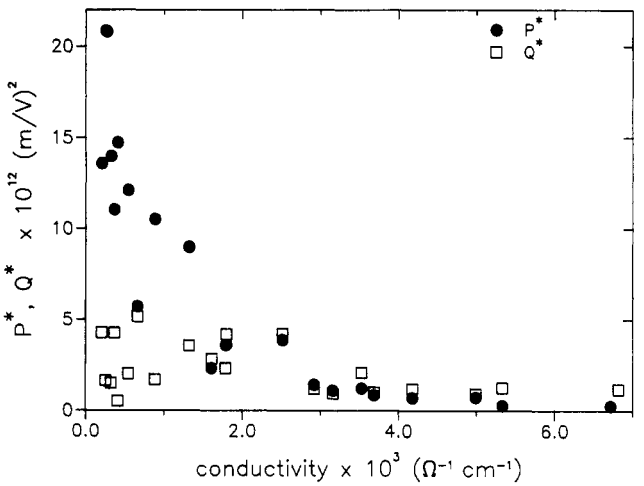

Figure 10. P^* and Q^* of LMM, determined from the area method, versus conductivity.

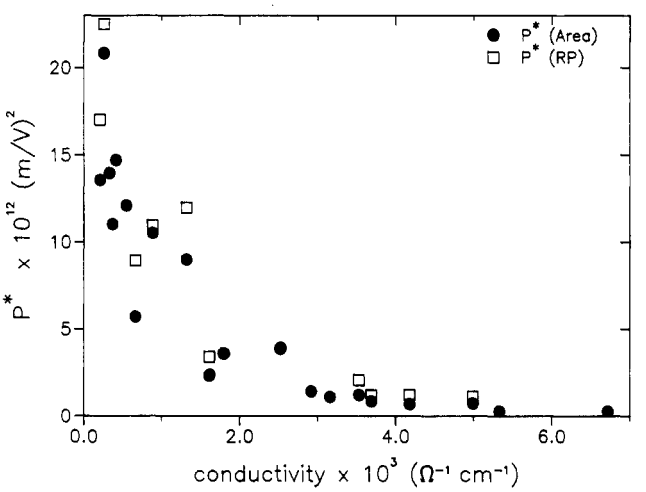

Figure 11. Comparison of the P^* of LMM determined by the area and RP methods, versus solution conductivity.

extrapolated to zero, was 3.84×10^{-6}. With Δn_s determined, an optical anisotropy factor of 1.55×10^{-3} was calculated using eq 9.

P^*/Q^* values were determined by the area method for each of the LMM samples shown in Figure 8. These values are shown in Table I and the errors shown are standard deviations of at least three area measurements. P^*/Q^* values were also obtained for some of the same LMM samples by the RP method and are also shown in Table I. For samples with no errors shown, only one reversing pulse measurement was possible. Only a limited number of reversing pulse measurements were possible because of unavoidable voltage spikes which were picked up by the detector during electric field reversal. These voltage spikes rendered many of the reversing pulse measurements useless. If it is assumed that $P^* = P$ and that $Q^* = Q$, then it is possible to calculate P, Q, μ, and $\alpha_1 - \alpha_2$ from the P^*/Q^* values obtained by either method; these values are also shown in Table I. The values of μ shown in Table I can be considered as the value of permanent dipole moment needed by the macromolecule in each experiment to explain the experimental data in the absence of slow ion atmosphere polarization. We shall, however, show that at least part of the experimentally observed values of P^* must arise from slow ion atmosphere polarization.

The conductivity dependence of the electrical terms P^* and Q^* determined from the area method are plotted in Figure 10. Between conductivity values of zero and 2.0×10^{-3} S cm^{-1}; Q^* fluctuates while at higher conductivity values it maintains a relatively constant value of approximately 1×10^{-12} $(m/V)^2$. Up to a conductivity value of 2.0×10^{-3} S cm^{-1}, P^* shows a decrease with increasing conductivity while at higher conductivity values P^* maintains a relatively constant value which is equivalent to Q^* in this conductivity range.

Figure 10 indicates that Q^* remained relatively constant, possibly decreasing slightly, with increasing conductivity. Evidently, however, P^* shows a significant decrease in value with increasing conductivity. Values of P^* determined by both the area

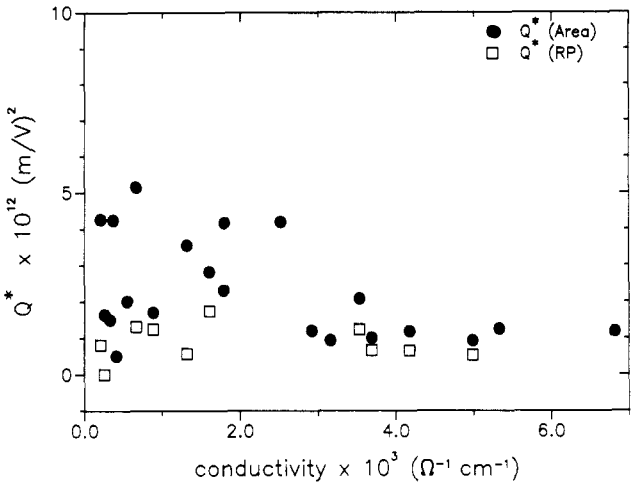

Figure 12. Comparison of the Q^* of LMM determined by the area and RP methods, versus solution conductivity.

method and the RP method can be compared at corresponding solution conductivities in Figure 11. It is evident from this figure that both methods for determining P^* show the same trend of a decrease in P^* with increasing conductivity. It is not known why P^* determined by the RP method was always greater than or equal to P^* determined by the area method. However, such differences have been noted in earlier unpublished work[34] on another muscle protein, paramyosin from the chowder clam, *Mercenaria mercenaria*. In that case, however, the values of P^* determined by the RP method were always less than those determined by the area method. Results like these probably highlight a defect in the theoretical treatments used. For example, eqs 19 and 20 were derived for insulating systems, but proteins have generally been studied in aqueous, somewhat conducting solutions. It will be seen below that, although some theoretical treatments of conducting solutions exist, none include both the transient effects *and* the steady-state effects in the same theoretical treatment.

Values of Q^* determined by both the area method and the RP method can be compared at corresponding solution conductivities on the graph in Figure 12. It can be seen in this figure that Q^* determined by the RP method always is less than Q^* determined by the area method.

Discussion

Generally, polyelectrolytes exhibit three kinds of electric moments.[44] The first is a permanent dipole moment, μ, and its relationship to P and K_{sp} is shown in eqs 6 and 7. The second is a field-induced dipole moment due to the distortion or polarization of the nuclear and electronic structure. This type of polarization of the macromolecule is expressed by the excess polarizability, $\alpha_1 - \alpha_2$, and its relationship to Q and K_{sp} are shown in eqs 6 and 8. The dipole moment from this kind of polarization will be referred to as the intrinsic induced dipole moment. The third kind of electric moment is also a field-induced dipole moment and is due to the redistribution or polarization of counterions over the polyelectrolyte surface.[9,45] The polarizability from this type of mechanism will be referred to as $\Delta\alpha$.

A number of workers have determined that the polarization of the ion atmosphere is frequency dependent.[1,33,46] Because of this, a relaxation time, τ_p, can be defined for the polarization of the ion atmosphere.[2,47] When this polarization relaxation time is much shorter than the transients in the applied electric field (the time it takes to first apply the electric field or the time needed for field reversal in our experiments) the dipole moment due to ion atmosphere polarization is called a fast induced dipole moment (FIDM). When this polarization relaxation time is of the order of or longer than the transients in the applied electric field, the dipole moment due to ion atmosphere polarization is called a slow induced dipole moment (SIDM). The implications of an SIDM and an FIDM are best understood if a polyelectrolyte is considered which has an intrinsic induced dipole moment and both an SIDM and an FIDM but no permanent dipole moment. This polyelectrolyte would have a birefringence rise time longer than its decay time and it would exhibit a field reversal transient. This polyelectrolyte would thus exhibit nonzero values of both P^* and Q^*, but steady-state measurements would show a zero value for P and a value of $Q > Q^*$. This polyelectrolyte would therefore orient in an electric field as if it were a macromolecule with both a permanent and intrinsic induced dipole moment. Thus, in fact, there are a total of four different orientation mechanisms possible for a polyelectrolyte. The first two are due to the permanent dipole moment and the intrinsic induced dipole moment of the polyelectrolyte. The other two possible orientation mechanisms are due to an SIDM and an FIDM. The orientation of a polyelectrolyte in an electric field may be due to any combination of these four orientation mechanisms. It is important to note that the orientation of a polyelectrolyte due to either a permanent dipole moment or an SIDM or both will result in a nonzero electrical term, P^*, that contributes to the transient response of the system to rapid changes in the electric field as in the rise of the birefringence and in field reversal experiments. However, only the permanent dipole moment contributes as a P term to the steady-state Kerr constant, K_{sp}, while the SIDM contributes as an induced dipole term, Q, to the K_{sp} of the macromolecule. In addition, the orientation of a polyelectrolyte due to an induced dipole moment or an FIDM or both will result in a nonzero electrical term, Q, contributing to the K_{sp} of the macromolecule.

Some workers[2,46] have shown using TEB that the polarization of the ion atmosphere in the form of an SIDM is important in explaining the orientation of DNA in an electric field. For example, DNA has shown a transient in the birefringence signal using a reversing pulse[2,46] which is often taken to indicate that a macromolecule has a permanent dipole moment. However, since DNA does not have a permanent dipole moment, the orientation of DNA in an electric field was best explained by invoking an SIDM.[2,46]

Let us now examine the nature of the electrical term, P^*, of LMM as determined above. It was shown, using Figure 10, that an increase in the ion concentration, or more appropriately, an increase in the ionic strength of the solution caused a decrease in P^*. Since LMM may have a true permanent dipole moment, it must be considered how a change in the ionic strength of the solution will affect both the permanent dipole moment and the SIDM. If LMM has a permanent dipole moment, a change in the ionic strength of the solution should have little or no effect on it assuming that it is due to the covalent structure of LMM. LMM may also have a permanent dipole moment due to charge anisotropy. If P^* is due mostly to charge anisotropy, the variation of P^* with ionic strength implies that the concentration of bound, immobile ions on LMM changes as a function of the ionic strength of the solution. This is possible, but large changes in charge anisotropy with ionic strength seem unlikely. A knowledge of the complete amino acid sequence in rabbit skeletal LMM should eventually allow this possibility to be explored.

The value of P or P^* due to a permanent dipole moment should decrease with increasing solution conductivity if one considers the changes in the reaction field of the dipole as the solution conductivity changes. Such changes were considered by O'Konski and Krause[9] who derived a theoretical treatment for the K_{sp} of rigid, dipolar, conducting ellipsoidal macromolecules in conducting solutions. In this treatment, the ion atmosphere polarization is described by defining an effective volume conductivity, κ_j (j = 1, 2 for ellipsoids of revolution), of the macromolecule. κ_j is the sum of a true volume conductivity, κ_j^0, and a term κ'_j which is a volume conductivity equivalent to a true surface conductivity. κ_j is therefore expressed by

$$\kappa_j = \kappa_j^0 + \kappa'_j \qquad (21)$$

κ_j^0 represents conduction in the chain structure of the macro-

(44) Yamaoka, K.; Kukudome, K. *J. Phys. Chem.* **1988**, *92*, 4994.
(45) Rau, D. C.; Charney, E. *Biophys. Chem.* **1981**, *14*, 1.
(46) Lewis, R. J.; Pecora, R.; Eden, D. *Macromolecules* **1987**, *20*, 2579.
(47) Morita, A.; Watanabe, H. *Macromolecules* **1984**, *17*, 1545.

molecule and κ'_j represents conduction on the surface of the chain structure. For polyelectrolytes, κ_j^0 is generally assumed to be zero[48] so that the effective volume conductivity, κ_j, of the polyelectrolyte is due to the surface conductivity term, κ'_j.

To a first approximation O'Konski and Krause[9] assumed that the surface conductivity of a polyelectrolyte arises mainly from the movement of mobile counterions on the surface of the macromolecule. O'Konski[49] calculated the surface conductivity term along the symmetry axis of a cylindrical rod to be

$$\kappa_1 = \frac{nzue}{2\pi ab^2} \tag{22}$$

where n is the total number of counterions of valence z, u is the mobility of the counterions, e is the electron charge, and a and b are the half-length and half-diameter of the rod. The surface conductivity term along the transverse axis is[49]

$$\kappa_2 = \kappa_1/2 \tag{23}$$

In order to incorporate the effect of a surface conductivity on the K_{sp} of a macromolecule, O'Konski and Krause[9] derived expressions for the electrical terms, P and Q, based on a dilute solution of ellipsoids of arbitrary and anisotropic volume conductivities, and dielectric constants, and carrying a permanent dipole moment. In order to simplify the expression for P, one can assume that the permanent dipole moment is directed along the symmetry axis of the molecule. With this assumption, the expression for P, considering the reaction field of the dipole is

$$P_1 = B_1^2(\kappa_1)\frac{{\mu_1}^2}{k^2T^2} \tag{24}$$

$B_1(\kappa_1)$ is an internal field function which is expressed as

$$B_1(\kappa_1) = \frac{1}{1 + \left(\frac{\kappa_1}{\kappa_s} - 1\right)A_1} \tag{25}$$

κ_s is the conductivity of the solvent and A_1 is a shape-dependent depolarization factor of the ellipsoid.[47] The expression for Q is

$$Q_{12} = \frac{V\epsilon_s\epsilon_0}{kT}\left[\left(\frac{\kappa_1}{\kappa_s} - \frac{\epsilon_1}{\epsilon_s}\right)B_1^2(\kappa_1) - \left(\frac{\kappa_2}{\kappa_s} - \frac{\epsilon_2}{\epsilon_s}\right)B_2^2(\kappa_2) + \left(\frac{\kappa_1}{\kappa_s} - 1\right)B_1(\kappa_1) - \left(\frac{\kappa_2}{\kappa_s} - 1\right)B_2(\kappa_2)\right] \tag{26}$$

V is the volume of the macromolecule, ϵ_s is the dielectric constant of the solvent, and ϵ_0 is the vacuum permittivity constant. ϵ_1 and ϵ_2 are the dielectric constants of the macromolecule along the symmetry and transverse axis, respectively. $B_2(\kappa_2)$ is similar to eq 25 for $B_1(\kappa_1)$ except that κ_1 is replaced by κ_2 and A_1 is replaced by A_2. The K_{sp} of a macromolecule with an effective volume conductivity can then be calculated using eq 6 with P and Q determined from eqs 24 and 26. The Q of eq 26 is a steady-state value that includes *both* the FIDM *and* the SIDM.

Using the theoretical treatment of O'Konski and Krause,[9] values of P, Q, and K_{sp} of LMM were calculated using the length of LMM as 715 Å as determined in the present work and the diameter as 20 Å. Using these dimensions, the calculated volume is 2.25×10^{-19} cm^3, assuming a right circular cylinder. Using an axial ratio of 36, A_1 and A_2 were assumed to be approximately equal to 0.0035 and 0.4982, respectively. These values of A_1 and A_2, which were previously reported,[49] are actually for an axial ratio of 30. However, since A_2 approaches an asymptotic value of 0.5 for large axial ratios, and since a small difference in A_1 will not significantly change the calculation using eq 25, the assumed values of A_1 and A_2 above are reasonable. The dielectric constant of the solvent was assumed to be equal to the dielectric constant of water, 78.5, and ϵ_1 and ϵ_2 were assumed to be equal to 4, the approximate macroscopic dielectric constant of polyamides.[50] A permanent dipole moment equal to 1000 D was assumed as a possibility for some of the calculations. This value is of the order of magnitude of the values calculated in Table I. In order to estimate κ_1 and κ_2, an approximation of the net charge on LMM is necessary. Since LMM has an isoelectric point of 4.8,[51] LMM probably has a net negative charge at a pH of 9, the approximate pH of the LMM solutions studied in the present work. As an initial guess, the net charge on LMM was assumed to be −10 so that n in eq 22 equals 10. The counterions were assumed to be K^+ ions with a mobility equal to 7.62×10^{-4} cm^2 s^{-1} V^{-1},[52] the mobility of K^+ ions in an infinitely dilute KCl solution at 25 °C. This mobility value will be referred as u. With this mobility, u, κ_1 equals 0.542 S cm^{-1} and κ_2 equals 0.271 S cm^{-1}. It was also assumed that LMM does not contribute to the bulk conductivity of the solution. This assumption is reasonable since no difference in solution conductivity between solutions with and without LMM could be detected in the present work.

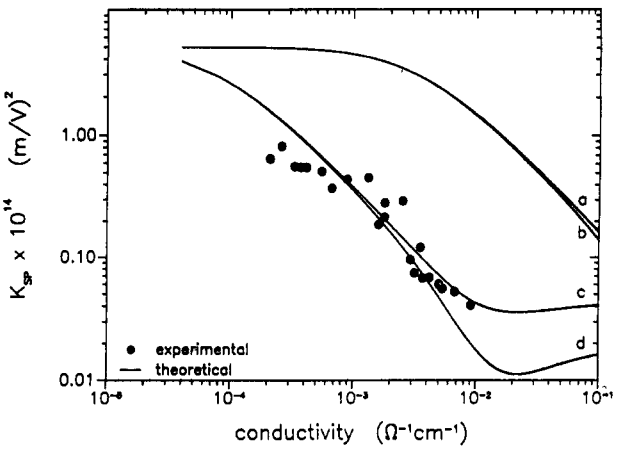

Figure 13. log K_{sp} of LMM versus solution conductivity. The theoretical curves were calculated using the O'Konski–Krause treatment[9] with the following parameters in which the K^+ mobility, u, is equal to its infinite dilution value. (a) Dipole moment 1000 D, K^+ mobility, u. (b) No dipole moment, K^+ mobility, u. (c) Dipole moment 1000 D, K^+ mobility, $u/45$. (d) No dipole moment, K^+ mobility, $u/45$.

Using the estimated parameters above, K_{sp} of LMM was predicted at the solution conductivities shown by curve a in Figure 13. Curve b in Figure 13 shows the effect of removing the permanent dipole moment from the calculations. Also plotted in Figure 13 are the experimental data from the present work. Curves a and b display a decrease in K_{sp} of LMM with increasing solution conductivity in agreement with the experimental data, but the experimental values are approximately 5 times smaller than the theoretical values from curves a and b. In order to calculate theoretical values of K_{sp} of LMM which are approximately equal to the magnitude of the experimental values, the mobility of the K^+ ions can be assumed to be 45 times less than mobility, u, of the K^+ ions used above. It is reasonable to assume that the mobility of ions on the surface of a polyelectrolyte is less than the mobility of the same ions in an infinitely dilute solution. Also, although the mobility of ions in solution generally decreases with an increase in ionic strength, these counterions are assumed to be close to the surface of the protein and the change of their mobility with ionic strength is unknown and was not estimated. Therefore, this reduced mobility, assumed constant at all the ionic strengths calculated, was used to predict the K_{sp} for LMM with and without a permanent dipole moment of 1000 D; the theoretical values using these parameters are shown by curves c and d, respectively, in Figure 13. Curves c and d in Figure 13 are equally good fits to the experimental data; this shows that permanent

(48) Krause, S.; Zvilichovsky, B.; Galvin, M. E. *Biophys. J.* **1980**, *29*, 413.
(49) O'Konski, C. T. *J. Phys. Chem.* **1960**, *64*, 605.
(50) *CRC Handbook of Chemistry and Physics*, 60th ed.; Weast, R. C., Astle, M. J., Eds.; CRC Press: Boca Raton, FL, 1979; p E-60.
(51) Hvidt, S.; Ferry, J. D.; Roelke, D. L.; Greaser, M. L. *Macromolecules* **1983**, *16*, 740.
(52) Harned, H. S.; Owen, B. B. *The Physical Chemistry of Electrolytic Solutions*; Reinhold Publishing Corp.: New York, 1958, p 228.

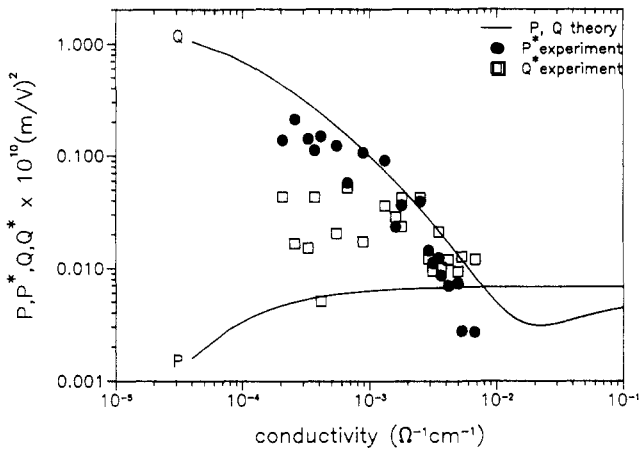

Figure 14. P^* and Q^* of LMM, determined by the area method versus conductivity. The theoretical curves of P and Q were calculated using the O'Konski–Krause treatment[9] using dipole moment 1000 D and K^+ mobility $u/45$, where u is the infinite dilution value.

dipole moments up to at least 1000 D do not change the predicted K_{sp} for this molecule using the O'Konski and Krause theory.[9] These curves were obtained using a charge of −10 and a counterion mobility 1/45 of the infinite dilution mobility of the K^+ counterions; the same results would be obtained using other negative charges for LMM with appropriate changes in the assumed counterion mobility. For example, if a charge of −30 is assumed, the mobility of the K^+ counterions needs to be reduced only by a factor of 15 in order to obtain the same results. At a solution conductivity of approximately 10^{-2} S cm^{-1} and larger, the inclusion of a permanent dipole moment in the theoretical calculations yields slightly larger K_{sp} values.

The experimental data for K_{sp} of LMM at the solution conductivities shown are reasonably fitted by the theoretical curves c and d. However, the P and Q values which contribute to the theoretical K_{sp} values shown in Figure 13 must also be compared to the experimental P^* and Q^* values. Figure 14 shows these theoretical P and Q values from eqs 24 and 26 together with the experimental P^* and Q^* values determined for LMM in the present work. The experimental P^* values agree fairly well with the theoretical Q values while the experimental Q^* values agree with no theoretical values on this plot. This implies that the theoretically calculated Q values, in which a very low mobility was used for the K^+, may be appearing in the form of experimental P^* values, that is, as SIDM's. As stated above, an SIDM will appear as a P^* in the transient behavior of the solution and it is the transient behavior of the solution that was used to determine the experimental values of P^*. The same SIDM, however, will appear as a Q factor in the steady-state behavior of the solution, that is, in the K_{sp}. The likelihood of an SIDM appears also in the greatly reduced mobility of the K^+ ions needed for the calculations as long as reasonable values of the charge on LMM are assumed, indicating that the polarization of the ion atmosphere is quite slow. It has been shown[53] that an SIDM which arises from ion atmosphere polarization can appear, experimentally, just like a permanent dipole moment in the rise of the birefringence and in the field reversal transient. This was done by Szabo and co-workers,[53] who derived a theoretical treatment for the polarization of an ion atmosphere which is coupled to the orientation of a macromolecule. They[53] defined a single relaxation time for the ion atmosphere, τ_P, which is equal to σ^2/D, where σ was defined as the average displacement between the centers of the counterion and polyelectrolyte charge distributions and D was defined as the surface diffusion constant of the counterion, collectively. When $\tau_P/\tau \gg 1$, the birefringence rise curve and the field reversal transient look exactly like those for a molecule with a large permanent dipole moment. Szabo et al.,[53] using TEB data for DNA, were able to analyze these data to find a value for τ_P, in their case, 0.12 μs for a 124 base pair DNA with birefringence relaxation time, τ, equal to 1.3 μs. They were able to do this because DNA has no permanent dipole moment. Furthermore, Wesenberg and Vaughan[54] were able to estimate the surface diffusion constant of a counterion from the above value of τ_P.

The molecule studied in this work, LMM, may have a permanent dipole moment, and it is possible that such a permanent dipole moment contributes to the experimentally determined P^* values, that is, to the birefringence rise curve and to the field reversal transient. In principle, it should be possible to determine whether a permanent dipole moment or an SIDM is the chief contributor to the field reversal transient. Tinoco and Yamaoka[33] showed that the time, t_m, from the moment of field reversal to the extremum in the field reversal birefringence transient, was

$$t_m = 1.5\tau \ln 3 \tag{27}$$

when the field reversal transient is due entirely to a permanent dipole moment, whereas

$$t_m = \frac{\tau_P \ln (\tau_P/\tau)}{(\tau_P/\tau) - 1} \tag{28}$$

for $\tau \neq \tau_P$ when the field reversal transient is due to an SIDM in the absence of a permanent dipole moment. Although it was possible for us to determine t_m for 9 of the 10 reversing pulses from Table I, these values, which ranged from 6.1 to 14.2 μs, should not be taken too seriously because of the voltage spikes, already mentioned earlier, which marred most of our RP measurements. On analyzing using eq 27, we obtain values of τ ranging from 3.7 to 8.6 μs, while eq 28 yields values of τ_P ranging from 6 to 51 μs (using the value τ = 5.8 μs determined from the field-free birefringence decay). Considering the uncertainties in our t_m values and the possibility that LMM has *both* a permanent dipole moment *and* an SIDM, we can only say that the analysis of our t_m values leads to no further conclusions. Furthermore, we did not attempt a point by point comparison of our birefringence transients with the theoretical treatments available. Szabo et al.[53] have shown that the Tinoco and Yamaoka treatment[33] does not give the correct transient response for a pure SIDM, but their own treatment does not include a permanent dipole moment.

Turning back to the variation of the experimentally determined value of Q^* of LMM with solution conductivity determined in the present work, let us reexamine the Q^* versus solution conductivity plot in Figure 10. There seems to be a small decrease in Q^* with an increase in solution conductivity, but it is also possible to conclude that Q^* does not change with changes in solution conductivity. Thus, an average value for Q^* = (2.28 ± 1.40) × 10^{-12} m^2 V^{-2} may be calculated in this conductivity range. It therefore seems as if Q^* depends only on the intrinsic induced dipole moment of LMM and that no FIDM exists. Using the average value of Q^* equals Q in eq 8, an average excess polarizability, $\alpha_1 - \alpha_2$, of (0.771 ± 0.470) × 10^{-16} cm^3 for LMM was calculated. This average excess polarizability can be compared to the excess polarizability calculated using the Peterlin and Stuart[22] theoretical treatment of electrically anisotropic ellipsoids of revolution. Their treatment assumes that Q depends on an intrinsic induced dipole moment only. The excess polarizability expressed by Peterlin and Stuart[22] is

$$\alpha_1 - \alpha_2 = v(g_{e1} - g_{e2}) \tag{29}$$

where v is the volume of the macromolecule and $g_{e1} - g_{e2}$ is an electrical anisotropy factor. This electrical anisotropy factor is expressed in a similar manner to the optical anisotropy factor (eq 10) with dielectric constants substituted for the respective refractive indices squared in eq 10. ϵ_1, ϵ_2, and ϵ_0 were assumed to be 4, 4, and 78.5, respectively, as was explained earlier in this section. Using these substitutions in eq 10, the electrical anisotropy factor equals 486. Using this value in eq 29 with the previously calculated volume of 2.25 × 10^{-19} cm^3 gives an excess polarizability of 1.09 × 10^{-16} cm^3. This calculated excess polarizability is in reasonable

(53) Szabo, A.; Haleem, M.; Eden, D. *J. Chem. Phys.* **1986**, *85*, 7472.

(54) Wesenberg, G. E.; Vaughan, W. E. *J. Chem. Phys.* **1987**, *87*, 4240.

agreement with the average excess polarizability of 0.771×10^{-16} cm^3 determined in the present work. Based on this agreement, it is likely that the Q^* values measured for LMM in the present work are due almost entirely to an intrinsic induced dipole moment. There is a problem with this analogy, because the theoretical treatment of O'Konski and Krause[9] should have included the intrinsic polarizability. If, however, the intrinsic polarizability is as much faster than the ion atmosphere polarizability as it seems from this work, it may contribute to Q^* in a decoupled fashion.

Conclusions

1. Although the steady state specific Kerr constant versus conductivity data on monomeric LMM can be made to fit the O'Konski/Krause[9] theoretical treatment, the individual variations of the P (the permanent dipole term) and Q (the induced dipole term) do not agree with the experimentally derived quantities P^* and Q^* which were determined using transient birefringence data.

2. However, the experimentally determined values of P^* agree rather well with the same theoretically calculated values of Q that give agreement with the specific Kerr constants. In order to calculate these values of Q it was necessary to use an exceptionally low value for the mobility of the counterions. This implies that the calculated values of Q were actually estimates of a slow induced dipole moment that acted experimentally like a permanent dipole moment.

3. The experimentally determined average value of Q^* is close to the value that can be calculated using the Peterlin-Stuart[22] theory which determines only intrinsic induced polarization.

4. The electric polarization mechanism of LMM consists mainly of a slow induced dipole moment connected with ion atmosphere polarization with an added contribution from the intrinsic induced dipole moment. The molecule may also have a permanent dipole moment.

Acknowledgment. We thank the National Science Foundation, Structural Chemistry and Thermodynamics Program, for Grant No. CHE-8308089 in partial support of this work. We also thank W. F. Harrington and M. E. Rodgers for allowing J.F.C. to help in the preparation of myosin and LMM at Johns Hopkins University.

Characterization of a Four-Component Cationic Reversed Micellar System: Dodecyltrimethylammonium Chloride/Hexanol/*n*-Heptane and 0.1 M KCl Solution

Christophe Petit,[†] Andreas S. Bommarius,[‡] Marie-Paule Pileni,*[,†] and T. Alan Hatton*[,‡]

Laboratoire de Structure et Reactivite aux Interfaces, Université de Paris VI, 75231 Paris Cedex 05, France, Department de Physico-Chimie, BP 121 Centre d'Etudes Nucleaires de Saclay, 91191 Gif-sur-Yvette Cedex, France, and Department of Chemical Engineering, Massachusetts Institute of Technology, Cambridge, Massachusetts 02139 *(Received: July 18, 1991; In Final Form: January 2, 1992)*

The reversed micellar region of the phase diagram for the DTAC/hexanol/*n*-heptane/buffer system has been characterized in terms of microemulsion droplet interfacial composition and size over a wide range of water-to-surfactant ratios, w_0. Phase boundary titration, conductivity, SAXS, and QELS measurements are all consistent with each other, giving strong support for the existence of a somewhat polydisperse dispersion of spherical droplets in the organic continuum stabilized by an interfacial cosurfactant-surfactant mixture of constant composition.

Introduction

Reversed micellar systems have attracted considerable attention recently owing to their ability to host various hydrophilic components in organic solvents, thereby providing a versatile environment for carrying out a range of reactions and separations.[1] The majority of investigations with reversed micelles have been carried out with three-component systems consisting of oil, surfactant, and an aqueous solution, which can be relatively easily characterized as to the limit of the reversed micellar region in the phase diagram, the micellar core, and hydrodynamic sizes as functions of water content, and the intermicellar interactions. The best known example of such a system is the anionic surfactant sodium bis(2-ethylhexyl) sulfosuccinate (Aerosol OT or AOT), a hydrocarbon as oil, and water. The behavior of four-component reversed micellar systems is more complex, as in addition to surfactant, oil, and an aqueous component, these systems also contain a cosurfactant, usually a medium-chain alcohol, which can act as a cosolvent as well. While there has been some work done on systems of this type,[2] in general they are less well characterized than the AOT system. Good characterization is a prerequisite for understanding changes in rate (i.e., kinetic and transport) and partitioning phenomena in reversed micellar systems with respect to their properties.

In this paper, we present a partial characterization of a cationic four-component reversed micellar system with the surfactant dodecyltrimethylammonium chloride (DTAC), hexanol as cosurfactant and cosolvent, *n*-heptane, and 0.1 M aqueous KCl solution at neutral pH. This system solubilizes water up to high molar water-surfactant ratios w_0, a property lacking in many reversed micellar systems but important for investigations of rate and partitioning phenomena in microheterogeneous systems. The system investigated here and similar ones have been used by us in the investigation of an enzymatic reaction sequence and of reversed micellar coalescence and redispersion processes,[3] and by Hilhorst et al. in a study of a coupled enzyme system involving cofactor regeneration.[4] The importance of having a well-characterized cationic reversed micellar system comparable to the well-known anionic AOT system for fundamental solute parti-

* Authors to whom correspondence should be addressed.
[†] Université de Paris VI and Centre d'Etudes Nucleaires de Saclay.
[‡] Massachusetts Institute of Technology.

(1) Pileni, M. P., Ed. *Structure and Reactivity in Reverse Micelles*; Elsevier: Amsterdam, 1989.
(2) (a) Abillon, O.; Binks, B. P.; Otero, C.; Langevin, D.; Ober, R. *J. Phys. Chem.* **1988**, *92*, 4411. (b) Binks, B. P.; Meunier, J.; Langevin, D. *Prog. Polym. Sci.* **1989**, *79*, 208.
(3) (a) Bommarius, A. S.; Hatton, T. A.; Wang, D. I. C. Manuscript in preparation. (b) Bommarius, A. S.; Holzwarth, J. F.; Wang, D. I. C.; Hatton, T. A. *J. Phys. Chem.* **1990**, *94*, 7232.
(4) (a) Hilhorst, R.; Spruijt, R.; Laane, C.; Veeger, C. *Eur. J. Biochem.* **1984**, *144*, 459. (b) Hilhorst, R. Ph.D. Thesis, Agricultural University; Wageningen, The Netherlands.

0022-3654/92/2096-4653$03.00/0